

Measurement of the $\gamma p \rightarrow K^0 \Sigma^+$ reaction with the Crystal Ball/TAPS detectors at the Mainz Microtron

P. Aguar-Bartolomé¹, J. R. M. Annand², H. J. Arends¹, K. Bantawa³, R. Beck⁴, V. Bekrenev⁵, H. Berghäuser⁶, A. Braghieri⁷, W. J. Briscoe⁸, J. Brudvik⁹, S. Cherepnaya¹⁰, R. F. B. Codling², C. Collicott^{11,12}, B. Demissie⁸, M. Dieterle¹³, E. J. Downie^{1,8}, P. Drexler⁶, L. V. Fil'kov¹⁰, A. Fix¹⁴, D. I. Glazier¹⁵, R. Gregor⁶, D. Hamilton², E. Heid^{1,8}, D. Hornidge¹⁶, D. Howdle², L. Isaksson¹⁷, I. Jaegle¹³, O. Jahn¹, T. C. Jude¹⁵, V. L. Kashevarov^{1,10}, I. Keshelashvili¹³, R. Kondratiev¹⁸, M. Korolija¹⁹, M. Kotulla⁶, A. Koulbardi⁵, S. Kruglov⁵, B. Krusche¹³, V. Lisin¹⁸, K. Livingston², I. J. D. MacGregor², Y. Maghrbi¹³, J. Mancel², D. M. Manley³, E. F. McNicoll², D. Mekterovic¹⁹, V. Metag⁶, A. Mushkarenkov⁷, B. M. K. Nefkens⁹, A. Nikolaev⁴, R. Novotny⁶, M. Oberle¹³, H. Ortega¹, M. Ostrick^{1*}, P. Ott¹, P. B. Otte¹, B. Oussena^{1,8}, P. Pedroni⁷, F. Pheron¹³, A. Polonski¹⁸, S. Prakhov^{8,9†}, J. Robinson², G. Rosner², T. Rostomyan¹³, S. Schumann¹, M. H. Sikora¹⁵, D. I. Sober²⁰, A. Starostin⁹, I. I. Strakovsky⁸, I. M. Suarez⁹, I. Supek¹⁹, C. M. Tarbert¹⁵, M. Thiel⁶, A. Thomas¹, M. Unverzagt^{1,4}, D. P. Watts¹⁵, D. Werthmüller¹³, L. Witthauer¹³, and F. Zehr¹³

(A2 Collaboration at MAMI)

¹*Institut für Kernphysik, Johannes Gutenberg-Universität Mainz, D-55099 Mainz, Germany*

²*SUPA, School of Physics and Astronomy, University of Glasgow, Glasgow G12 8QQ, United Kingdom*

³*Kent State University, Kent, Ohio 44242-0001, USA*

⁴*Helmholtz-Institut für Strahlen- und Kernphysik, University of Bonn, D-53115 Bonn, Germany*

⁵*Petersburg Nuclear Physics Institute, 188350 Gatchina, Russia*

⁶*II Physikalisches Institut, University of Giessen, D-35392 Giessen, Germany*

⁷*INFN Sezione di Pavia, I-27100 Pavia, Italy*

⁸*The George Washington University, Washington, DC 20052-0001, USA*

⁹*University of California Los Angeles, Los Angeles, California 90095-1547, USA*

¹⁰*Lebedev Physical Institute, 119991 Moscow, Russia*

¹¹*Dalhousie University, Halifax, Nova Scotia B3H 4R2, Canada*

¹²*Saint Mary's University, Halifax, Nova Scotia B3H 3C3, Canada*

¹³*Institut für Physik, University of Basel, CH-4056 Basel, Switzerland*

¹⁴*Laboratory of Mathematical Physics, Tomsk Polytechnic University, 634050 Tomsk, Russia*

¹⁵*SUPA, School of Physics, University of Edinburgh, Edinburgh EH9 3JZ, United Kingdom*

¹⁶*Mount Allison University, Sackville, New Brunswick E4L 1E6, Canada*

¹⁷*Lund University, SE-22100 Lund, Sweden*

¹⁸*Institute for Nuclear Research, 125047 Moscow, Russia*

¹⁹*Rudjer Boskovic Institute, HR-10000 Zagreb, Croatia and*

²⁰*The Catholic University of America, Washington, DC 20064, USA*

(Dated: September 26, 2018)

The $\gamma p \rightarrow K^0 \Sigma^+$ reaction has been measured from threshold to $E_\gamma = 1.45$ GeV ($W_{\text{CM}} = 1.9$ GeV) using the Crystal Ball and TAPS multiphoton spectrometers together with the photon tagging facility at the Mainz Microtron MAMI. In the present experiment, this reaction was searched for in the $3\pi^0 p$ final state, by assuming $K_S^0 \rightarrow \pi^0 \pi^0$ and $\Sigma^+ \rightarrow \pi^0 p$. The experimental results include total and differential cross sections as well as the polarization of the recoil hyperon. The new data significantly improve empirical knowledge about the $\gamma p \rightarrow K^0 \Sigma^+$ reaction in the measured energy range. The results are compared to previous measurements and model predictions. It is demonstrated that adding the present $\gamma p \rightarrow K^0 \Sigma^+$ results to existing data allowed a better description of this reaction with various models.

PACS numbers: 13.60.-r, 13.60.Hb, 13.88.+e

I. INTRODUCTION

The unique extraction of partial-wave scattering amplitudes and universal baryon-resonance parameters from

experimental data as well as their precise interpretation in QCD ranks among the most challenging tasks in modern hadron physics. During the last decades, an enormous effort to study baryon resonances in photoinduced meson production at various laboratories has started. Many single- and double-spin observables for different final states have been measured for the first time.

*corresponding author; e-mail: ostrick@kph.uni-mainz.de

†corresponding author; e-mail: prakhov@ucla.edu

Photoinduced kaon-hyperon (KY) production has attracted much attention for two reasons. First, open

strangeness production necessarily involves the generation of a strange $q\bar{q}$ pair, and new aspects of nucleon spectroscopy might be discovered, which are not manifest in reactions containing pion-nucleon initial or final states. Second, the weak hyperon decays reveal the polarization state of the final-state baryon. This information is essential in order to achieve a model-independent amplitude reconstruction in a so-called complete experiment [1, 2].

The basic reactions include $\gamma p \rightarrow K^+\Lambda$, $\gamma p \rightarrow K^+\Sigma^0$, and $\gamma p \rightarrow K^0\Sigma^+$, as well as the corresponding reactions off the neutron. The production of an isoscalar Λ hyperon involves only N^* resonances, while $\gamma p \rightarrow K^+\Sigma^0$ and $\gamma p \rightarrow K^0\Sigma^+$ may receive contributions from both N^* and Δ^* states. Therefore, an experimentally based isospin decomposition of the transition amplitudes requires data on both reactions with similar quality.

Differential cross sections and hyperon polarization for reactions with a charged kaon, $\gamma p \rightarrow K^+\Lambda$ and $\gamma p \rightarrow K^+\Sigma^0$, were measured at Jefferson Lab using the CLAS detector [3–5], at ELSA using the SAPHIR detector [6, 7], at GRAAL [8], and with LEPS [9, 10]. Recent measurements of the beam-recoil observables with CLAS [11] and GRAAL [12] are important steps toward a model-independent amplitude reconstruction.

The $\gamma p \rightarrow K^0\Sigma^+$ reaction can be identified via the decays $K_S^0 \rightarrow \pi^0\pi^0$ or $K_S^0 \rightarrow \pi^+\pi^-$ and $\Sigma^+ \rightarrow \pi^0 p$ or $\Sigma^+ \rightarrow \pi^+ n$. Differential cross sections have been measured by CBELSA/TAPS, using the $\pi^0\pi^0\pi^0 p$ final state [13, 14], and by SAPHIR [15, 16] and CLAS [17], using the $\pi^+\pi^-\pi^0 p$ and $\pi^+\pi^-\pi^+ n$ final states. Compared to the $K^+\Lambda$ and $K^+\Sigma^0$ channels, the statistical accuracy of the existing $K^0\Sigma^+$ data are rather limited, especially at energies below $E_\gamma = 1.5$ GeV.

In parallel with these experimental efforts, a lot of theoretical studies for modeling and understanding the dynamics of kaon photoproduction were started. Calculations have been performed in the framework of single- or multichannel isobar models [18–20], coupled-channel approaches [21–23] as well as chiral-unitary approaches [24]. It turned out that, in contrast to single π or η photoproduction, both resonant and nonresonant contributions play an almost equally important part in the reaction dynamics. Therefore, extracted resonance parameters strongly depend on the treatment of the nonresonant contributions and a conclusive picture about the dynamics and the baryon-resonance contributions has not yet been achieved.

In the phenomenological KAON-MAID model [18], the nonresonant part of the amplitudes contains s -, u -, and t -channel terms along with a contact interaction, which is required to restore gauge invariance after hadronic form factors are introduced. The model was fitted to the first SAPHIR $\gamma p \rightarrow K^+\Lambda$, $\gamma p \rightarrow K^+\Sigma^0$ [6], and $\gamma p \rightarrow K^0\Sigma^+$ data [15]. In the Regge-Plus-Resonance (RPR) approach of Refs. [19, 25], modeling nonresonant contributions via exchange of Regge trajectories involves only a few parameters, which can be constrained by the high-energy data above the resonance region. The latest

Bonn-Gatchina (BnGa) partial-wave analysis (PWA) [20] incorporates the majority of existing data from pion- and photoinduced reactions into simultaneous multichannel fits. In Ref. [24], a unitary, gauge-invariant coupled-channel approach based on a chiral effective Lagrangian was used to describe the threshold regions of kaon photoproduction without including any resonances at all.

This work reports on new experimental results for the $\gamma p \rightarrow K^0\Sigma^+$ reaction that include total and differential cross sections and recoil polarization of Σ^+ . The data were obtained with the Crystal Ball/TAPS multiphoton spectrometers, using the energy-tagged beam of bremsstrahlung photons from the Mainz Microtron. Compared to the previous experiments, the present statistics and the quality of the data allow us to measure the $\gamma p \rightarrow K^0\Sigma^+$ reaction at $E_\gamma < 1450$ MeV with a higher accuracy and smaller energy binning.

II. EXPERIMENTAL SETUP

The reaction $\gamma p \rightarrow K^0\Sigma^+$ was measured using the Crystal Ball (CB) [26] as the central spectrometer and TAPS [27, 28] as a forward spectrometer. These detectors were installed in the energy-tagged bremsstrahlung photon beam of the Mainz Microtron (MAMI) [29, 30]. The photon energies are determined by the Glasgow tagging spectrometer [31–33].

The CB detector is a sphere consisting of 672 optically isolated NaI(Tl) crystals, shaped as truncated triangular pyramids, which point toward the center of the sphere. The crystals are arranged in two hemispheres that cover 93% of 4π sr, sitting outside a central spherical cavity with a radius of 25 cm, which is designed to hold the target and inner detectors. In this experiment, TAPS was arranged in a plane consisting of 384 BaF₂ counters of hexagonal cross section. It was installed 1.5 m downstream of the CB center and covered the full azimuthal range for polar angles from 1° to 20°. More details on the energy and angular resolution of the CB and TAPS are given in Refs. [34, 35].

The present measurement used 1508- and 1557-MeV electron beams from the upgraded Mainz Microtron, MAMI-C [30]. The data with the 1508-MeV beam were taken in 2007 and those with the 1557-MeV beam in 2009. Bremsstrahlung photons, produced by the 1508-MeV electrons in a 10- μ m Cu radiator and collimated by a 4-mm-diameter Pb collimator, were incident on a 5-cm-long liquid hydrogen (LH₂) target located in the center of the CB. The energies of the incident photons were analyzed up to 1402 MeV by detecting the post-bremsstrahlung electrons in the Glasgow tagger [31]. With the 1557-MeV electron beam, the incident photons were analyzed up to 1448 MeV, and a 10-cm-long LH₂ target was used. The energy resolution of the tagged photons is mostly defined by the width of tagger focal-plane detectors and by the electron-beam energy. For the present beam energies, a typical width of a tagger chan-

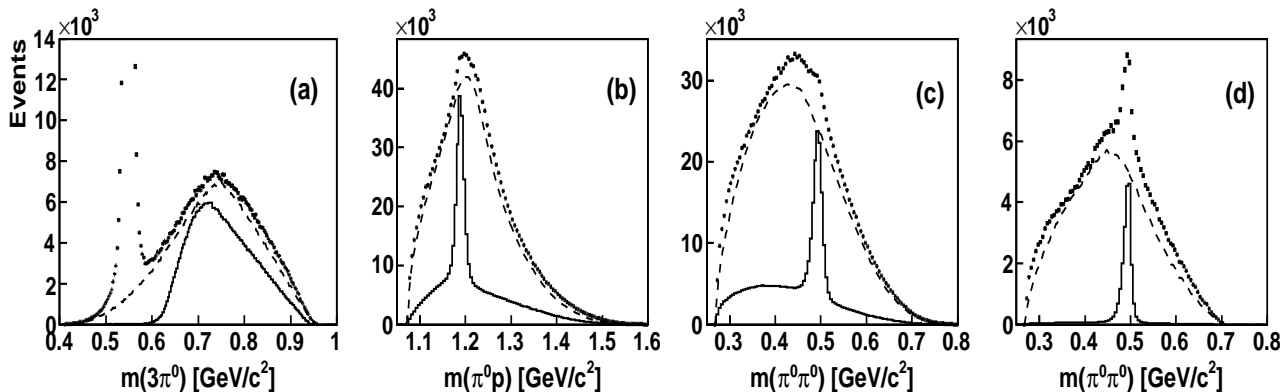


FIG. 1: Comparison of the invariant-mass distributions (a) $m(3\pi^0)$, (b) $m(\pi^0 p)$, and (c) and (d) $m(\pi^0\pi^0)$, obtained for the experimental $\gamma p \rightarrow 3\pi^0 p$ events (crosses) and for the MC simulation of $\gamma p \rightarrow K^0\Sigma^+ \rightarrow 3\pi^0 p$ (solid line) and $\gamma p \rightarrow 2\pi^0\Delta^+(1232) \rightarrow 3\pi^0 p$ (dashed line). All distributions are obtained for events above the $\gamma p \rightarrow K^0\Sigma^+$ threshold. The $m(\pi^0 p)$ and $m(\pi^0\pi^0)$ distributions are obtained for $m(3\pi^0) > 0.6 \text{ GeV}/c^2$. The events in (d) are selected by testing the $\gamma p \rightarrow \pi^0\pi^0\Sigma^+ \rightarrow 3\pi^0 p$ hypothesis.

nel was about 4 MeV. Due to the beam collimation, only part of the bremsstrahlung photon flux reached the LH₂ target. In order to extract the reaction cross sections, the probability of bremsstrahlung photons reaching the target (the so-called tagging efficiency) was measured for each tagger channel. The average tagging efficiency in the experiment with the 1508-MeV electron beam was found to vary from 69% at the $\gamma p \rightarrow K^0\Sigma^+$ threshold to 64% at $E_\gamma = 1.4 \text{ GeV}$. With the 1557-MeV electron beam, the average tagging efficiency was similar to the 1508-MeV-beam magnitudes up to $E_\gamma = 1.4 \text{ GeV}$, dropping then to 57% at $E_\gamma = 1.45 \text{ GeV}$.

The experimental trigger in the measurement with the 1508-MeV electron beam required two conditions: 1. the total-energy deposited in the CB had to exceed $\sim 320 \text{ MeV}$ and 2. the number of so-called hardware clusters in the CB (multiplicity trigger) had to be larger than two. With the 1557-MeV electron beam, the trigger on the total energy in the CB was increased to $\sim 340 \text{ MeV}$. TAPS was not in the multiplicity trigger for these experiments.

More details on the experimental conditions of the data taking with the 1508-MeV electron beam in 2007 are given in Refs. [34, 35].

III. DATA HANDLING

The reaction $\gamma p \rightarrow K^0\Sigma^+$ was searched for in the $3\pi^0 p$ final state, by assuming $K_S^0 \rightarrow \pi^0\pi^0$ and $\Sigma^+ \rightarrow \pi^0 p$. The $\gamma p \rightarrow 3\pi^0 p \rightarrow 6\gamma p$ candidates were extracted from the analysis of events having six and seven clusters reconstructed in the CB and TAPS together. As reported in Ref. [35], a large part of the $3\pi^0 p$ final state comes from the process $\gamma p \rightarrow \eta p \rightarrow 3\pi^0 p$. However, this process can be easily separated from $\gamma p \rightarrow K_S^0\Sigma^+$ based on

the invariant mass of the $3\pi^0$ system, which is heavier than the η mass for $\gamma p \rightarrow K_S^0\Sigma^+$ events. Another part of $\gamma p \rightarrow 3\pi^0 p$ is the so-called direct $3\pi^0$ production that comes from processes involving only a chain of N^* and Δ^* decays.

Besides the physical $3\pi^0$ background, there are two more background sources. The first one comes from interactions of incident photons in the windows of the target cell. The subtraction of this background from the experimental spectra was based on the analysis of the data samples that were taken with an empty (no liquid hydrogen) target. Another background is due to random coincidences of the tagger hits with the experimental trigger; its subtraction was done by using only those tagger hits for which all coincidences were random (see Refs. [34, 35] for more details).

The selection of event candidates was based on the kinematic-fit technique. The details of the kinematic-fit parametrization of the detector information and resolution are given in Ref. [34]. The hypothesis $\gamma p \rightarrow 3\pi^0 p \rightarrow 6\gamma p$ was tested to identify all events that have the $3\pi^0 p$ final state. The events that satisfied this hypothesis at the 2% confidence level (CL) (i.e., with a probability of misinterpretation less than 2%) were accepted as the reaction candidates. The kinematic-fit output for which the pairing combination of the six photons to the three π^0 s had the largest CL was used to reconstruct the reaction kinematics. The hypothesis $\gamma p \rightarrow \eta p \rightarrow 3\pi^0 p \rightarrow 6\gamma p$ was tested to identify those events that were produced via the $\eta \rightarrow 3\pi^0$ decay. The test of the hypothesis $\gamma p \rightarrow K^0\Sigma^+ \rightarrow 3\pi^0 p \rightarrow 6\gamma p$ was not done as it would accept all direct $3\pi^0 p$ events that have a combination of the invariant masses of the $\pi^0 p$ and $\pi^0\pi^0$ systems simultaneously close to the mass of Σ^+ and K^0 .

The determination of the experimental acceptance was based on a Monte Carlo (MC) simulation of the $\gamma p \rightarrow$

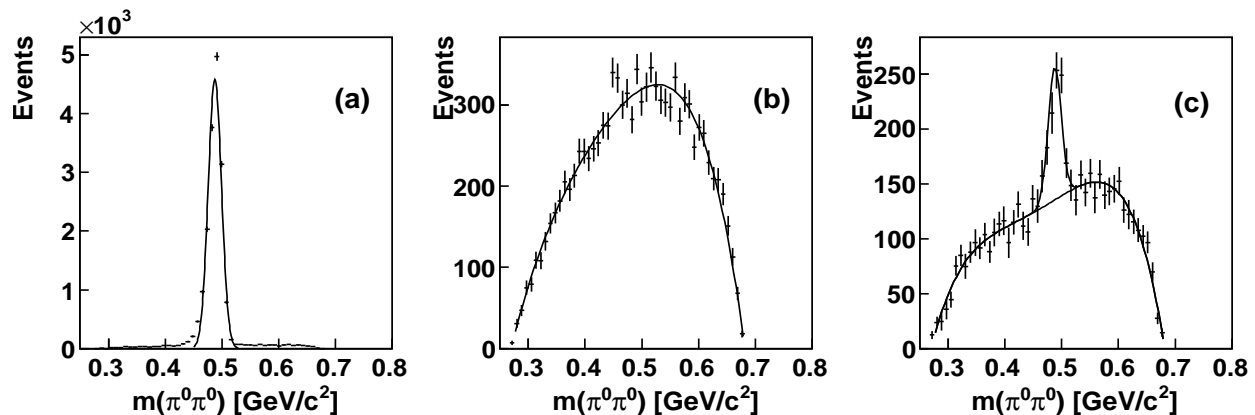


FIG. 2: The $m(\pi^0\pi^0)$ distributions for (a) the MC simulation of $\gamma p \rightarrow K^0\Sigma^+ \rightarrow 3\pi^0 p$ with a Gaussian fit, (b) the MC simulation of $\gamma p \rightarrow 2\pi^0\Delta^+(1232) \rightarrow 3\pi^0 p$ with a fit of a polynomial of order five, and (c) the experimental data fitted with the sum of a Gaussian and a polynomial of order five.

$K^0\Sigma^+ \rightarrow 3\pi^0 p$ reaction with an isotropic production angular distribution. Two background reactions were simulated as $\gamma p \rightarrow \eta p \rightarrow 3\pi^0 p$ and $\gamma p \rightarrow 2\pi^0\Delta^+(1232) \rightarrow 3\pi^0 p$, also with isotropic production angular distributions. For the data at each electron-beam energy, the corresponding MC events were propagated through a GEANT (version 3.21) simulation of the experimental setup. To reproduce resolutions of the experimental data, the GEANT output (energy and timing) was subject to additional smearing, thus allowing both the simulated and experimental data to be analyzed in the same way. The simulated events were also tested for whether they passed the trigger requirements.

In Fig. 1, various invariant-mass distributions obtained from the experimental $\gamma p \rightarrow 3\pi^0 p$ events are compared to those obtained from the MC simulation of the processes $\gamma p \rightarrow K^0\Sigma^+ \rightarrow 3\pi^0 p$ and $\gamma p \rightarrow 2\pi^0\Delta^+(1232) \rightarrow 3\pi^0 p$. All events are plotted only for beam energies above the $\gamma p \rightarrow K^0\Sigma^+$ threshold (~ 1048 MeV). The $3\pi^0$ invariant-mass distributions are depicted in Fig. 1(a). As seen, the experimental distribution includes a strong peak from $\gamma p \rightarrow \eta p \rightarrow 3\pi^0 p$ events and a structure that is similar to the MC simulation of $\gamma p \rightarrow 2\pi^0\Delta^+(1232) \rightarrow 3\pi^0 p$. Also, one can see that events from $\gamma p \rightarrow K^0\Sigma^+ \rightarrow 3\pi^0 p$ and $\gamma p \rightarrow \eta p \rightarrow 3\pi^0 p$ barely overlap. The $\pi^0 p$ invariant-mass distributions are shown in Fig. 1(b) for events with $m(3\pi^0) > 0.6$ GeV/c^2 . The corresponding invariant mass for the $\pi^0\pi^0$ system is shown in Fig. 1(c). These distributions for $m(\pi^0 p)$ and $m(\pi^0\pi^0)$ have three entries per one event because of the number of final-state π^0 s. As seen in Fig. 1(b), the experimental $m(\pi^0 p)$ spectrum reveals a clear signal from the $\Delta^+(1232) \rightarrow \pi^0 p$ decay, the shape of which is close to the MC simulation of $\gamma p \rightarrow 2\pi^0\Delta^+(1232) \rightarrow 3\pi^0 p$. As a weak signal from $\Sigma^+(1189) \rightarrow \pi^0 p$ sits on a big bump from $\Delta^+(1232) \rightarrow \pi^0 p$, this makes it difficult to use the $m(\pi^0 p)$ distribution for fitting the Σ^+ signal above background. As seen in Fig. 1(c), the $\pi^0\pi^0$ background under

the $K_S^0 \rightarrow \pi^0\pi^0$ signal is much smoother. The shape of this background is also close to the MC simulation of $\gamma p \rightarrow 2\pi^0\Delta^+(1232) \rightarrow 3\pi^0 p$. To enlarge the signal-to-background ratio in the $m(\pi^0\pi^0)$ distribution, only events from the region of the $\Sigma^+(1189)$ peak should be accepted into the $m(\pi^0\pi^0)$ distribution. The width of this peak can be determined from the MC simulation of $\gamma p \rightarrow K^0\Sigma^+ \rightarrow 3\pi^0 p$, which is shown in Fig. 1(b) by a solid line. Such an approach was used in the previous analyses of the CBELSA data [13, 14]. The present analysis revealed that an even better solution is to test the hypothesis $\gamma p \rightarrow \pi^0\pi^0\Sigma^+ \rightarrow 3\pi^0 p$ with the kinematic fit. Besides selecting events from the region of the $\Sigma^+(1189)$ peak, the use of this hypothesis also improves the angular resolution and the $m(\pi^0\pi^0)$ resolution for the actual $\gamma p \rightarrow K^0\Sigma^+ \rightarrow 3\pi^0 p$ events. Fitting the $\gamma p \rightarrow \pi^0\pi^0\Sigma^+ \rightarrow 3\pi^0 p$ hypothesis resulted in $\sigma = 3.4^\circ$ for the resolution in the K_S^0 polar angle in the center-of-mass (c.m.) frame and $\sigma = 8.6$ MeV/c^2 for the invariant-mass resolution of the two π^0 from the K_S^0 decay, whereas the corresponding values based on the fit of the $\gamma p \rightarrow 3\pi^0 p$ hypothesis were 3.6° and 11.0 MeV/c^2 . The results of fitting the $\gamma p \rightarrow \pi^0\pi^0\Sigma^+ \rightarrow 3\pi^0 p$ hypothesis are shown in Fig. 1(d). The $m(\pi^0\pi^0)$ distribution from the MC simulation of $\gamma p \rightarrow K^0\Sigma^+ \rightarrow 3\pi^0 p$ includes now an almost clean, narrower peak from $K_S^0 \rightarrow \pi^0\pi^0$. The K_S^0 signal in the experimental $m(\pi^0\pi^0)$ distribution is much more prominent than the one in Fig. 1(c).

All previous measurements of $\gamma p \rightarrow K^0\Sigma^+$ were made with wide energy bins; the smallest bins were 100-MeV wide. This prevented an adequate characterization of the region from threshold to the excitation-function maximum, causing difficulties with the theoretical interpretation of the data. The present data were divided into eight energy bins from $E_\gamma = 1050$ MeV to $E_\gamma = 1450$ MeV, allowing 50-MeV energy binning for measuring both the $\gamma p \rightarrow K^0\Sigma^+$ cross sections and recoil polarization of Σ^+ . The data within one energy bin were divided into six

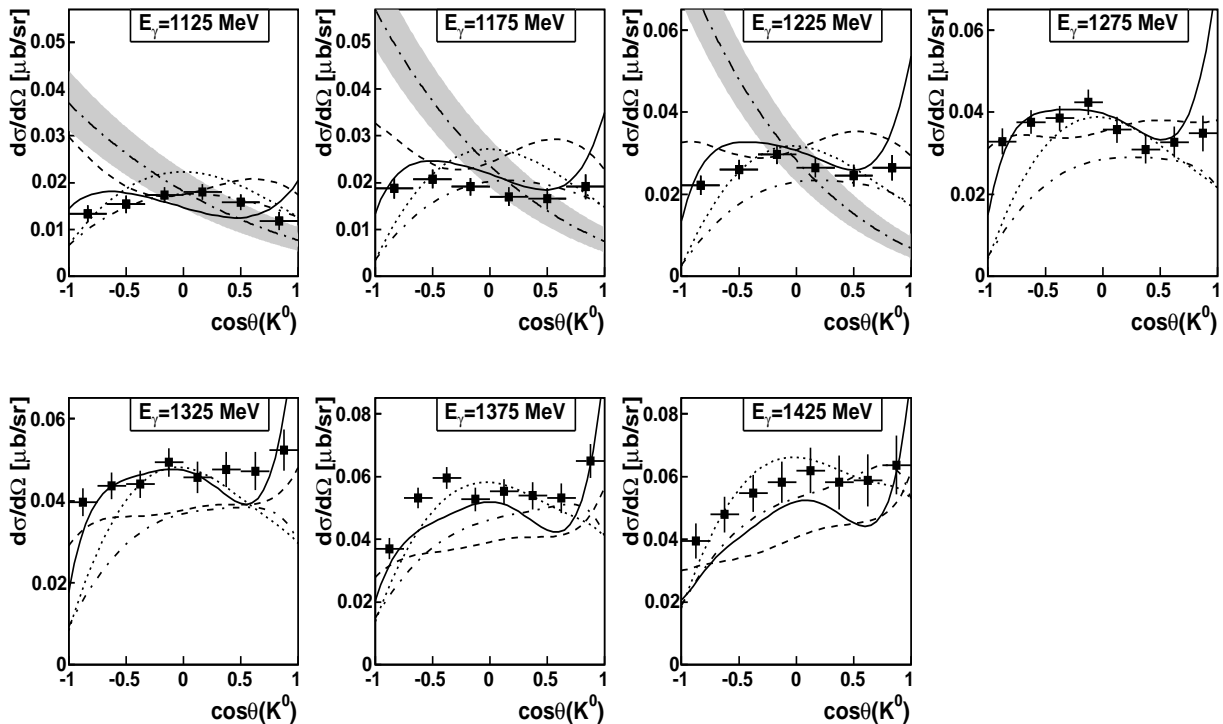


FIG. 3: $\gamma p \rightarrow K^0 \Sigma^+$ differential cross sections of this work (solid squares) compared to the predictions of various models: BG2011-2 (solid line), BG2011-1 (dashed line) [20], RPR-3 (dotted line) [19], RPR-A (dash-dotted line) [25], and chiral-unitary approach (long-dash-dotted line with gray error band) [24].

$\cos \theta$ bins for $E_\gamma < 1250$ MeV and into eight $\cos \theta$ bins for $E_\gamma > 1250$ MeV, where θ is the angle between the direction of the outgoing K^0 and the incident photon in the c.m. frame.

Although the 50-MeV binning covers entirely the energy range available in this experiment, unfortunately, the energy points themselves do not match any existing data. For a better comparison of the present and previous data, an additional set of results was obtained also with the use of 50-MeV bins, but with the energy points matching all previous measurements. Namely, the additional set includes five energy points: 1100, 1200, 1250, 1300, and 1400 MeV. This additional set was used only for illustration (Figs. 4 and 7) and cannot be used in any further analysis, as its results are strongly correlated with the results of the main set.

The $K_S^0 \rightarrow \pi^0 \pi^0$ signal was fitted individually in every $\cos \theta$ bin. The fitting procedure is illustrated in Fig. 2 for one particular energy and $\cos \theta$ bin. The $m(\pi^0 \pi^0)$ distribution from the MC simulation of $\gamma p \rightarrow K^0 \Sigma^+ \rightarrow 3\pi^0 p$ fitted with a Gaussian is shown in Fig. 2(a). The $m(\pi^0 \pi^0)$ distribution from the MC simulation of $\gamma p \rightarrow 2\pi^0 \Delta^+(1232) \rightarrow 3\pi^0 p$ fitted with a polynomial of order five is shown in Fig. 2(b). The experimental $m(\pi^0 \pi^0)$ distribution fitted with the sum of a Gaussian and a polynomial of order five is shown in Fig. 2(c). For the latter fit, the initial parameters for the polynomial were taken from the previous fit to the MC simulation of

$\gamma p \rightarrow 2\pi^0 \Delta^+(1232) \rightarrow 3\pi^0 p$, and two parameters of the Gaussian (namely, the mean value and σ) were fixed to the values from the previous fit to the MC simulation of $\gamma p \rightarrow K^0 \Sigma^+ \rightarrow 3\pi^0 p$. Since the calculation of the experimental number of $\gamma p \rightarrow K^0 \Sigma^+ \rightarrow 3\pi^0 p$ events was based on the area under the Gaussian, the corresponding detection efficiency was calculated in the same way (based on the area under the Gaussian fit to the MC simulation of $\gamma p \rightarrow K^0 \Sigma^+ \rightarrow 3\pi^0 p$).

The recoil polarization P of the Σ^+ hyperon was measured via its parity-violating weak decay $\Sigma^+ \rightarrow \pi^0 p$. The angular distribution of the decay nucleon is given by Ref. [36] as

$$W(\cos \xi_N) \sim 1 + \alpha P \cos \xi_N, \quad (1)$$

where $\alpha = -0.98$ is the asymmetry parameter for the $\Sigma^+ \rightarrow \pi^0 p$ decay. The angle ξ is defined by

$$\cos \xi = (\hat{\gamma} \times \hat{K}^0) \cdot \hat{n} / |\hat{\gamma} \times \hat{K}^0| = \hat{N} \cdot \hat{n}, \quad (2)$$

where $\hat{\gamma}$ and \hat{K}^0 are, respectively, vectors in the direction of the incident photon and the outgoing K^0 , \hat{n} is a unit vector in the direction of the decay proton in the Σ^+ rest frame, and \hat{N} is the normal to the production plane. Based on the decay asymmetry of Σ^+ with respect to the production plane, the polarization was measured by averaging the proton angular distribution above ($\cos \xi >$

TABLE I: Differential cross sections for $\gamma p \rightarrow K^0 \Sigma^+$ at the energies for which the data were divided into six $\cos \theta$ bins.

E_γ [MeV]	1125 \pm 25	1175 \pm 25	1225 \pm 25
$\cos \theta(K^0)$	$d\sigma/d\Omega$ [$\mu\text{b}/\text{sr}$]	$d\sigma/d\Omega$ [$\mu\text{b}/\text{sr}$]	$d\sigma/d\Omega$ [$\mu\text{b}/\text{sr}$]
-1.0 to -0.667	0.0133 \pm 0.0018	0.0188 \pm 0.0022	0.0221 \pm 0.0023
-0.667 to -0.333	0.0154 \pm 0.0019	0.0208 \pm 0.0020	0.0260 \pm 0.0023
-0.333 to 0.0	0.0174 \pm 0.0017	0.0191 \pm 0.0019	0.0296 \pm 0.0023
0.0 to 0.333	0.0180 \pm 0.0017	0.0170 \pm 0.0020	0.0265 \pm 0.0023
0.333 to 0.667	0.0158 \pm 0.0017	0.0166 \pm 0.0023	0.0246 \pm 0.0027
0.667 to 1.0	0.0118 \pm 0.0020	0.0191 \pm 0.0026	0.0265 \pm 0.0031

TABLE II: Differential cross sections for $\gamma p \rightarrow K^0 \Sigma^+$ at the energies for which the data were divided into eight $\cos \theta$ bins.

E_γ [MeV]	1275 \pm 25	1325 \pm 25	1375 \pm 25	1425 \pm 25
$\cos \theta(K^0)$	$d\sigma/d\Omega$ [$\mu\text{b}/\text{sr}$]			
-1.0 to -0.75	0.0329 \pm 0.0032	0.0396 \pm 0.0034	0.0371 \pm 0.0034	0.0395 \pm 0.0056
-0.75 to -0.5	0.0376 \pm 0.0029	0.0437 \pm 0.0033	0.0532 \pm 0.0033	0.0480 \pm 0.0057
-0.5 to -0.25	0.0385 \pm 0.0030	0.0441 \pm 0.0033	0.0596 \pm 0.0035	0.0547 \pm 0.0060
-0.25 to 0.0	0.0424 \pm 0.0031	0.0494 \pm 0.0035	0.0528 \pm 0.0038	0.0582 \pm 0.0066
0.0 to 0.25	0.0357 \pm 0.0031	0.0457 \pm 0.0038	0.0553 \pm 0.0039	0.0620 \pm 0.0073
0.25 to 0.5	0.0309 \pm 0.0035	0.0476 \pm 0.0042	0.0540 \pm 0.0044	0.0581 \pm 0.0086
0.5 to 0.75	0.0327 \pm 0.0038	0.0472 \pm 0.0046	0.0531 \pm 0.0047	0.0587 \pm 0.0083
0.75 to 1.0	0.0348 \pm 0.0043	0.0524 \pm 0.0051	0.0650 \pm 0.0054	0.0637 \pm 0.0094

0) and below ($\cos \xi < 0$) this plane:

$$P = \frac{2 N_{\text{up}} - N_{\text{down}}}{\alpha N_{\text{up}} + N_{\text{down}}}, \quad (3)$$

where N_{up} and N_{down} represent, respectively, the number of events with the decay proton emitted above and below the production plane.

IV. DISCUSSION OF THE RESULTS

The differential cross sections for $\gamma p \rightarrow K^0 \Sigma^+$ and recoil polarization of Σ^+ were obtained as a function of $\cos \theta_{K^0}$, where θ_{K^0} is the angle between the direction of K^0 and the incident photon in the c.m. frame. As discussed in Sec. III, the main results were obtained for eight 50-MeV intervals, covering the full energy range available in the experiment. Additional results were obtained just for a better comparison with existing data, also using 50-MeV intervals, but with the energy points matching the previous measurements.

Since the mean value and σ of the Gaussian were fixed while fitting to the experimental $m(\pi^0 \pi^0)$ spectra, the statistical uncertainties in the results for the differential cross sections and recoil polarization are based on the fit errors for the Gaussian height parameter. These uncertainties are shown in the figures and listed in the tables.

The systematic uncertainties in the results are more essential for the differential cross sections, and most of

them are canceled in the calculation of recoil polarization. The largest contribution to the systematic uncertainties comes from the parametrization of the background in the fits. According to our study, this uncertainty is about 0.003 $\mu\text{b}/\text{sr}$ for each individual value in the differential cross sections, independent of its magnitude. This uncertainty was estimated by changing the degree of a polynomial used in the fit and the $m(\pi^0 \pi^0)$ range fitted. Although for the largest values in the differential cross sections, this uncertainty is only about 5%, for the smallest values, it reaches 25%. The systematic uncertainty because of the combinatorial background under the peak from the $K_S^0 \rightarrow \pi^0 \pi^0$ decays (see Fig. 2(a)) is at the level of 1%–2%, depending on the $\cos \theta_{K^0}$ value. The overall systematic uncertainty that comes from the determination of the experimental acceptance with the MC simulation and from the calculation of the photon-beam flux is about 4%. This uncertainty for the $3\pi^0 p$ final state was studied by measuring the process $\gamma p \rightarrow \eta p \rightarrow 3\pi^0 p$, which has a much larger yield and little background, for the same data sets (see Ref. [35] for more details).

The results below $E_\gamma = 1400$ MeV are obtained as a weighted average of the results from the data with the 1508-MeV beam and with the 1557-MeV beam. The results obtained for the first energy bin, 1050–1100, are not very reliable because of a very weak $K^0 \Sigma^+$ signal above large background, so they are omitted in this work.

The results of our main set for the $\gamma p \rightarrow K^0 \Sigma^+$ differential cross sections are listed in Tables I and II. In

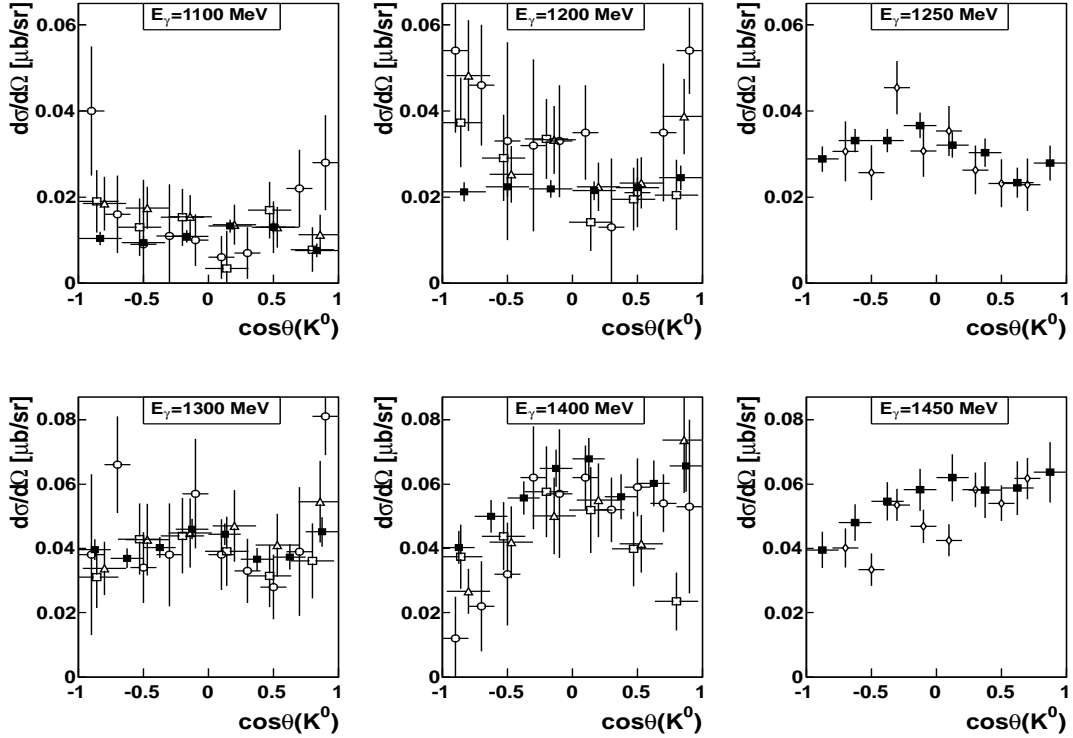


FIG. 4: $\gamma p \rightarrow K^0 \Sigma^+$ differential cross sections from the additional set of this work (solid squares), compared to the previous measurements: SAPHIR (open circles, 100-MeV bins) [16], CB-ELSA 2008 (open squares, 100-MeV bins) [13], CB-ELSA 2010 (open triangles, 100-MeV bins) [14], and CLAS (open diamonds, 200-MeV bins, with CLAS data at 1450 MeV being compared to the results of this work at an energy of 1425 MeV) [17].

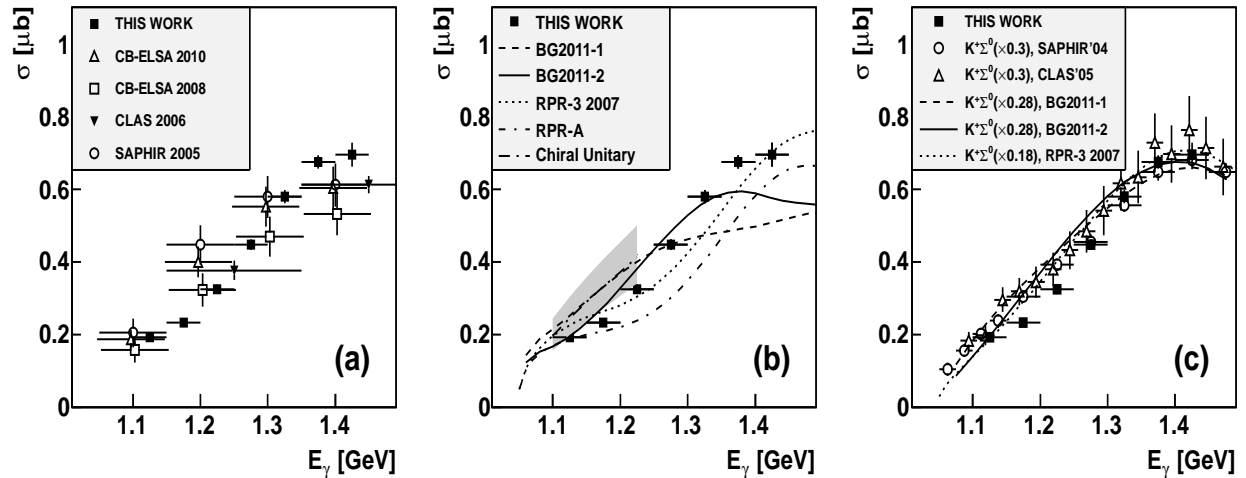


FIG. 5: $\gamma p \rightarrow K^0 \Sigma^+$ total cross sections of this work (solid squares) compared to (a) previous measurements by SAPHIR (open circles) [16], CLAS (solid triangles) [17] normalized to the full $\cos \theta_{K^0}$ range, CB-ELSA 2008 (open squares) [13], and CB-ELSA 2010 (open triangles) [14]; (b) predictions by BG2011-2 (solid line), BG2011-1 (dashed line) [20], RPR-3 (dotted line) [19], RPR-A (dash-dotted line) [25], and the chiral-unitary approach (long-dash-dotted line with gray error band) [24]; (c) the $\gamma p \rightarrow K^+ \Sigma^0$ total cross sections by SAPHIR 2004 (open circles; multiplied by a factor of 0.3) [7], CLAS 2006 (open triangles, $\times 0.3$) [4], BG2011-2 (solid line, $\times 0.28$), BG2011-1 (dashed line, $\times 0.28$), and RPR-3 (dotted line, $\times 0.18$)

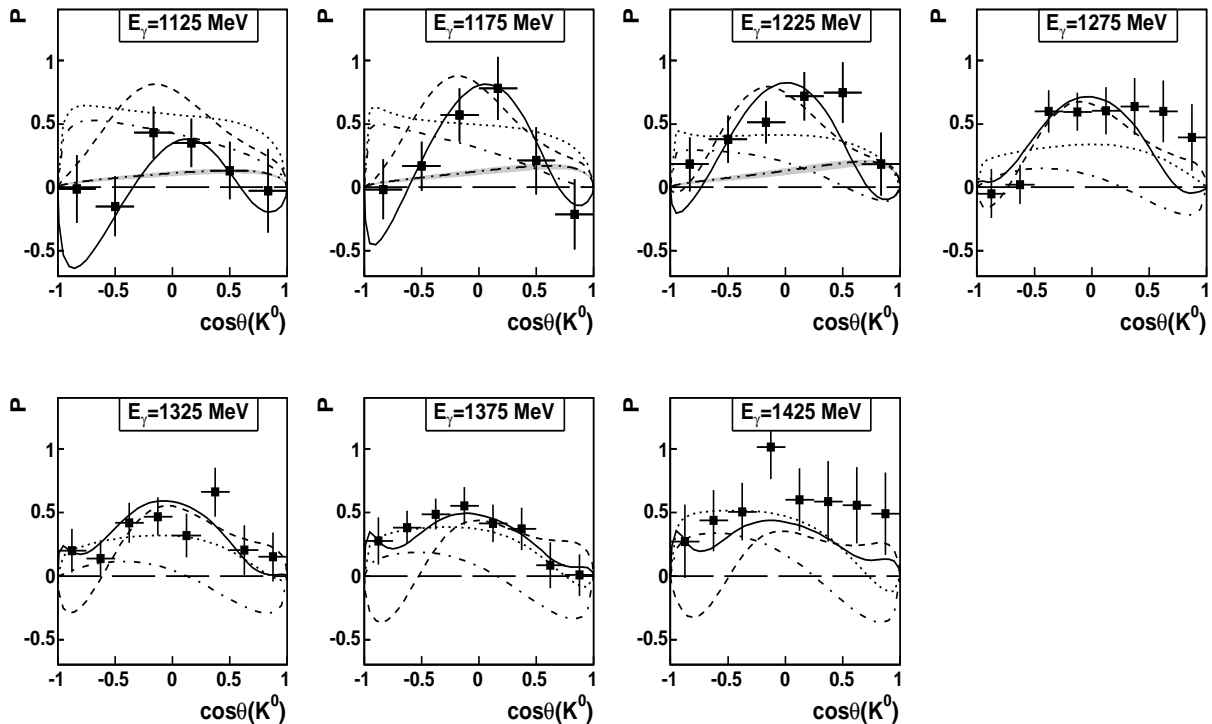


FIG. 6: Results of this work (solid squares) for recoil polarization of Σ^+ compared to predictions from the models BG2011-2 (solid line), BG2011-1 (dashed line), RPR-3 (dotted line), and RPR-A (dash-dotted line) and from the chiral-unitary approach (long-dash-dotted line with gray error band).

Fig. 3, these differential cross sections are compared to predictions of various models. The latest BnGa multi-channel PWA [20] permits two classes of solutions, called BG2011-1 (shown in the figures by a dashed line) and BG2011-2 (shown by a solid line). The RPR approach is presented by a solution with background model 3 (RPR-3) from Ref. [19] (shown by a dotted line) and a revised solution with background model 3 (RPR-A) from Ref. [25] (shown by a dash-dotted line). The gauge-invariant chiral-unitary approach is shown by a long-dash-dotted line with a gray error band. None of these predictions is in good agreement with the measured differential cross sections for the full energy range. The KAON-MAID predictions from Ref. [18] are not shown here as the model was fitted to the first SAPHIR data [6] (not shown here), in which the background was significantly underestimated. The chiral-unitary calculation of Ref. [24] does not describe the angular distributions. However, the order of magnitude of the cross section comes out correctly. This is already a success as no baryon resonance contributions are explicitly added in these calculations. As seen from the comparison, adding the present results to the existing data will require a revision of the analysis of photoinduced $K\Sigma$ production by all models.

In Fig. 4, the measured differential cross sections from the additional set of this work are compared to all recent data in this energy range. As seen, all previous

measurements are made for wider energy bins and have larger error bars. Although the error bars of the other data at $E_\gamma = 1100$ MeV and $E_\gamma = 1200$ MeV are much larger than the ones of this work, the present results appear to be smaller than the previous measurements, especially at the extreme angles. This hints that the background in those measurements was underestimated at these angles. The results of the CLAS Collaboration [17] at $E_\gamma = 1250$ MeV and $E_\gamma = 1450$ MeV are in good agreement within the error bars with the results of this work. The results obtained at $E_\gamma = 1300$ MeV and $E_\gamma = 1400$ MeV are in agreement within the error bars with the majority of the previous measurements.

The total cross sections for $\gamma p \rightarrow K^0 \Sigma^+$ were obtained by the integration of the present differential cross sections. In Fig. 5(a), these total cross sections are compared to the previous measurements. Since the differential cross sections of CLAS were obtained for a limited angular range only, their partial total cross sections were normalized by us to the ratio of the full and covered ranges of $\cos\theta_{K^0}$. As seen, although the previous results have larger error bars, which overlap with the present data points, the energy dependence of the measured cross sections shows a more steady rise from threshold to the maximum. In Fig. 5(b), the present total cross sections are compared to predictions from the models BG2011-1, BG2011-2, RPR-3, and RPR-A and from the chiral-unitary approach. As seen, the prediction from

TABLE III: Recoil polarization of Σ^+ at the energies for which the data were divided into six $\cos\theta$ bins.

E_γ [MeV]	1125 ± 25	1175 ± 25	1225 ± 25
$\cos\theta(K^0)$	P	P	P
-1.0 to -0.667	-0.013 ± 0.266	-0.017 ± 0.236	0.181 ± 0.212
-0.667 to -0.333	-0.149 ± 0.236	0.167 ± 0.194	0.380 ± 0.185
-0.333 to 0.0	0.431 ± 0.207	0.569 ± 0.211	0.513 ± 0.167
0.0 to 0.333	0.349 ± 0.190	0.780 ± 0.247	0.718 ± 0.191
0.333 to 0.667	0.133 ± 0.225	0.210 ± 0.265	0.745 ± 0.238
0.667 to 1.0	-0.026 ± 0.329	-0.212 ± 0.277	0.184 ± 0.250

TABLE IV: Recoil polarization of Σ^+ at the energies for which the data were divided into eight $\cos\theta$ bins.

E_γ [MeV]	1275 ± 25	1325 ± 25	1375 ± 25	1425 ± 25
$\cos\theta(K^0)$	P	P	P	P
-1.0 to -0.75	-0.050 ± 0.194	0.199 ± 0.172	0.274 ± 0.186	0.273 ± 0.289
-0.75 to -0.5	0.023 ± 0.155	0.135 ± 0.147	0.383 ± 0.129	0.436 ± 0.243
-0.5 to -0.25	0.596 ± 0.167	0.419 ± 0.157	0.486 ± 0.122	0.506 ± 0.226
-0.25 to 0.0	0.594 ± 0.150	0.469 ± 0.148	0.553 ± 0.149	1.018 ± 0.256
0.0 to 0.25	0.604 ± 0.186	0.318 ± 0.173	0.414 ± 0.147	0.601 ± 0.246
0.25 to 0.5	0.637 ± 0.226	0.660 ± 0.192	0.373 ± 0.167	0.588 ± 0.316
0.5 to 0.75	0.599 ± 0.244	0.204 ± 0.195	0.086 ± 0.181	0.557 ± 0.300
0.75 to 1.0	0.393 ± 0.264	0.150 ± 0.193	0.007 ± 0.164	0.490 ± 0.325

BG2011-2 is closer to the present data than BG2011-1, and the prediction from RPR-3 is closer than RPR-A. However, none of the predictions is sufficiently close to the present data. Compared to the previous measurements, the energy dependence of the present total cross sections is much closer to the corresponding energy dependence of the isospin-related reaction $\gamma p \rightarrow K^+\Sigma^0$. If both the reactions in this energy range were dominated by production via Δ^* states, the $\gamma p \rightarrow K^+\Sigma^0$ yield should be about four times as large, compared to $\gamma p \rightarrow K^0\Sigma^+$. To illustrate this similarity, in Fig. 5(c) the present $\gamma p \rightarrow K^0\Sigma^+$ cross sections are compared to the rescaled ones of $\gamma p \rightarrow K^+\Sigma^0$, which are represented by the CLAS [4] and SAPHIR [7] data and predictions from the models BG2011-1, BG2011-2, and RPR-3. As seen, the measured energy dependence for $\gamma p \rightarrow K^0\Sigma^+$ is very similar to that for $\gamma p \rightarrow K^+\Sigma^0$.

The results of our main set for recoil polarization of Σ^+ are listed in Tables III and IV. In Fig. 6, these results are compared to predictions from the models BG2011-1, BG2011-2, RPR-3, and RPR-A and from the chiral-unitary approach. In our opinion, the prediction from BG2011-2 is the closest one for most of the data, and the prediction from RPR-3 is better than RPR-A. The prediction from the chiral-unitary approach is much smaller than the experimental values. In Fig. 7, the recoil-polarization results from the additional set of this work are compared to all previous measurements in this energy range, which are represented by only four energies,

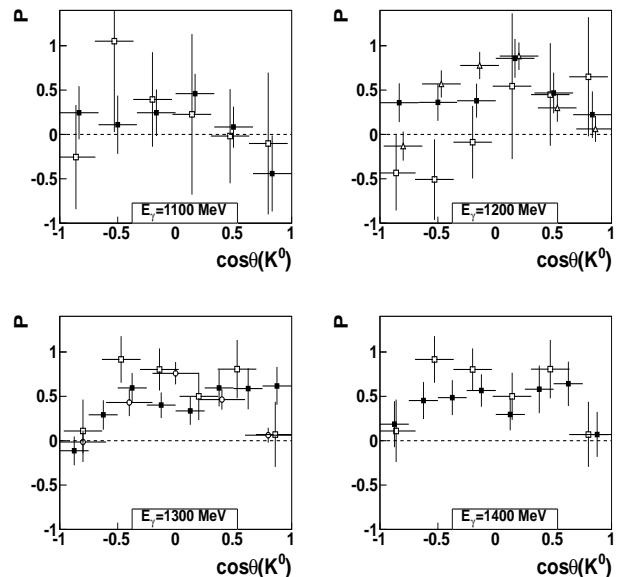


FIG. 7: Σ^+ recoil-polarization results from the additional set of this work (solid squares) compared to the previous measurements: SAPHIR (open circles, 250-MeV bins), CB-ELSA 2008 (open squares, 100-MeV bins), and CB-ELSA 2010 (open triangles, 150-MeV bins).

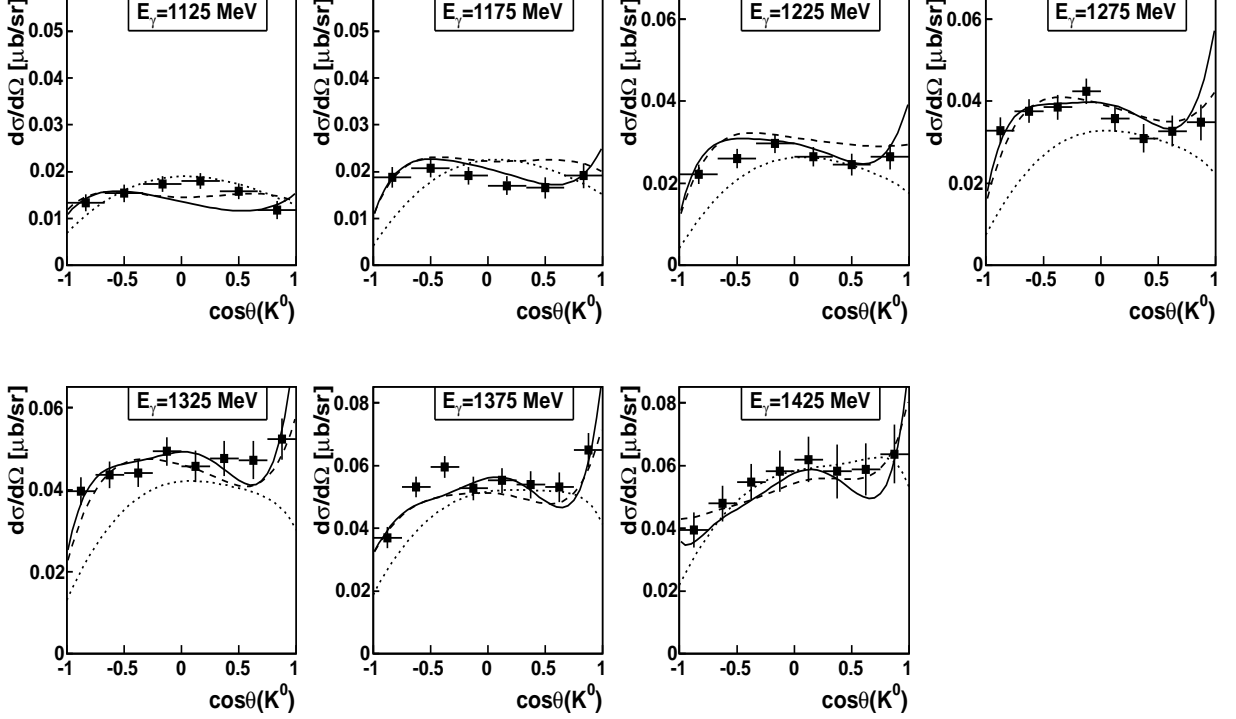


FIG. 8: $\gamma p \rightarrow K^0 \Sigma^+$ differential cross sections from this work (solid squares) compared to the predictions based on new fits of models: BG2011-2 (solid line), BG2011-1 (dashed line), and RPR-2007 (dotted line).

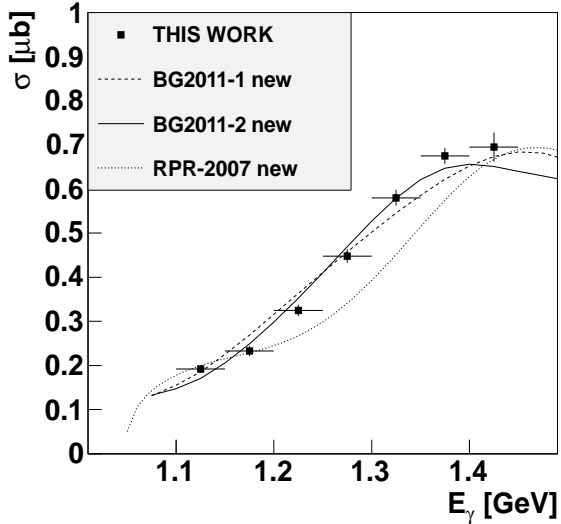


FIG. 9: $\gamma p \rightarrow K^0 \Sigma^+$ total cross sections from this work (solid squares) compared to the predictions based on new fits of models: BG2011-2 (solid line), BG2011-1 (dashed line), and RPR-2007 (dotted line).

with wider energy bins and larger uncertainties. As seen, for all four energies, the present results are in agreement within the error bars with the majority of the previous

measurements.

To check the importance of the present data for a better understanding of the $\gamma p \rightarrow K^0 \Sigma^+$ dynamics in our energy range, the RPR and BnGa groups added the results of this work in their analysis of $K \Sigma$ photoproduction. The revised results of their fits [37] are shown in Fig. 8 for the differential cross sections, in Fig. 9 for the total cross sections, and in Fig. 10 for recoil polarization of Σ^+ . As seen, the RPR-2007 approach, which is a revised RPR-3 model, gives a better prediction for the shape of the differential cross sections, but leaves a discrepancy for the total cross sections and recoil polarization. The RPR-A model was eliminated by the present data. For both the BG2011-1 and BG2011-2 solutions, the updated BnGa PWA yields results which are very close to the present $\gamma p \rightarrow K^0 \Sigma^+$ data, especially for higher photon energies. Both RPR and BnGa groups observed a strong influence from the present data on their analyses. Details for these results will be published by the RPR and BnGa groups separately [37].

V. SUMMARY AND CONCLUSIONS

The $\gamma p \rightarrow K^0 \Sigma^+$ reaction has been measured from threshold to $E_\gamma = 1.45$ GeV. The measurement was conducted by using the Crystal Ball and TAPS multiphoton spectrometers together with the Glasgow photon tagging

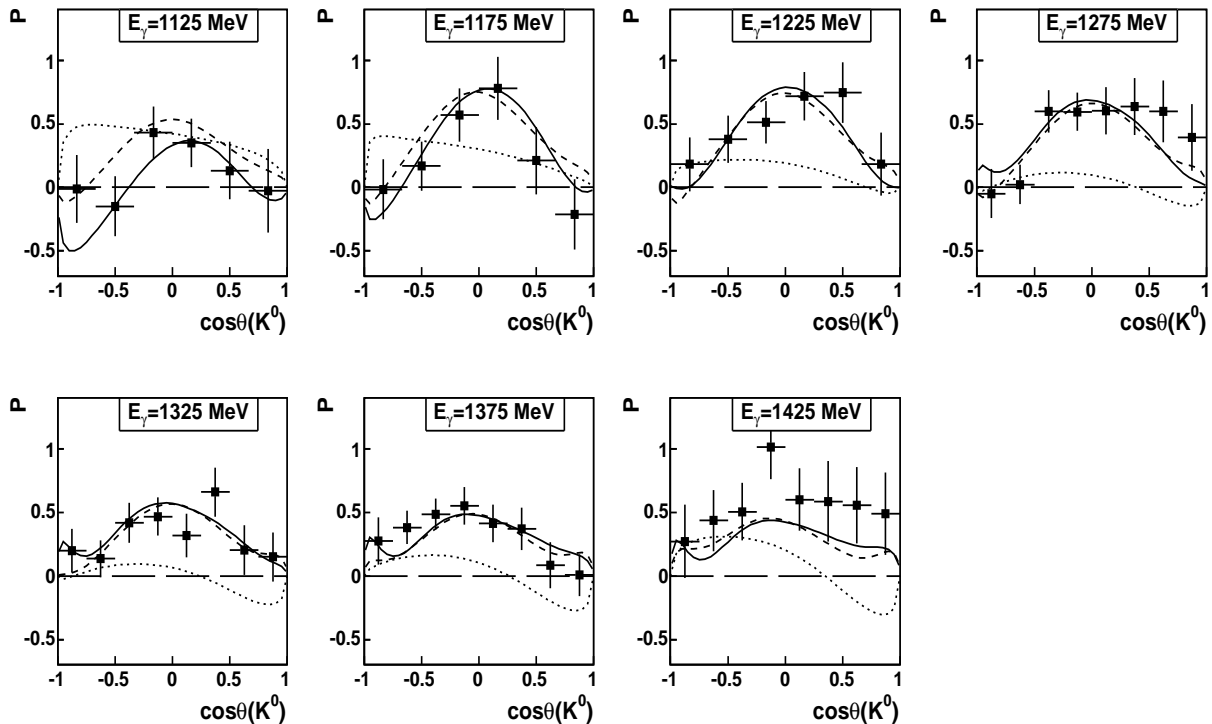


FIG. 10: Results of this work (solid squares) for recoil polarization of Σ^+ compared to predictions based on new fits of models: BG2011-2 (solid line), BG2011-1 (dashed line), and RPR-2007 (dotted line).

facility at the Mainz Microtron. The experimental results include total and differential cross sections and recoil polarization of Σ^+ . The comparison of the present results to previous measurements reveals generally good agreement. However, the data of this work are obtained for narrower energy bins and with smaller uncertainties. The accuracy of the results presented in this work allows a significant improvement of the world data base for the $\gamma p \rightarrow K^0 \Sigma^+$ reaction. The comparison of the present results to the existing model predictions indicates that none of them describes well the present data in the entire measured energy range. With these new data, different models can be restricted much more precisely, leading to a more accurate description of the $\gamma p \rightarrow K^0 \Sigma^+$ reaction.

Acknowledgment

The authors wish to acknowledge the excellent support of the accelerator group and operators of MAMI. We also

thank A. Sarantsev on behalf of the BnGa PWA group, P. Vancraeyveld and J. Ryckebusch on behalf of the RPR analysis groups, as well as P. Bruns for their help and constructive comments. This work was supported by the Deutsche Forschungsgemeinschaft (SFB443, SFB/TR16, and SFB1044), DFG-RFBR (Grant No. 09-02-91330), the European Community-Research Infrastructure Activity under the FP6 “Structuring the European Research Area” program (Hadron Physics, Contract No. RII3-CT-2004-506078), Schweizerischer Nationalfonds, the U.K. Science and Technology Facilities Council, the U.S. Department of Energy and National Science Foundation, and NSERC (Canada). A. Fix acknowledges additional support from the Russian Federation federal program “Kadry” (Contract No. P691) and the MSE Program “Nauka” (Contract No. 1.604.2011). We thank the undergraduate students of Mount Allison University and The George Washington University for their assistance.

-
- [1] I.S. Barker, A. Donnachie, J.K. Storrow, Nucl. Phys. B **95**, 347 (1975).
 [2] A.M. Sandozi *et al.*, J. Phys. **38**, 053001 (2011).
 [3] J.W.C. McNabb *et al.*, Phys. Rev. C **69**, 042201 (2004).
 [4] R. Bradford *et al.*, Phys. Rev. C **73**, 035202 (2006).

- [5] B. Dey *et al.*, Phys. Rev. C **82**, 025202 (2010).
 [6] M.Q. Tran *et al.*, Phys. Lett. B **445**, 20 (1998).
 [7] K.-H. Glander *et al.*, Eur. Phys. J. A **19**, 251 (2004).
 [8] A. Lleres *et al.*, Eur. Phys. J. A **31**, 79 (2007).
 [9] M. Sumihama *et al.*, Phys. Rev. C **73**, 035214 (2006).

- [10] H. Kohri *et al.*, Phys. Rev. Lett. **97**, 082003 (2006).
- [11] R.K. Bradford *et al.*, Phys. Rev. C **75**, 035205 (2007).
- [12] A. Lleres *et al.*, Eur. Phys. J. A **39**, 149 (2009).
- [13] R. Castelijns *et al.*, Eur. Phys. J. A **35**, 39 (2008).
- [14] R. Ewald (for the CBELSA/TAPS Collaboration), AIP Conf. Proc. 1257, 566 (2010).
- [15] S. Goers *et al.*, Phys. Lett. B **464**, 331 (1999).
- [16] R. Lawall *et al.*, Eur. Phys. J. A **24**, 275 (2005).
- [17] F.J. Klein (for the CLAS Collaboration), Nucl. Phys. A **754**, 321 (2005).
- [18] T. Mart, C. Bemmhold, Phys. Rev. C **61**, 012201 (1999); www.kph.uni-mainz.de/MAID/kaon/kaonmaid.html
- [19] T. Corthals, T. Van Cauteren, J. Ryckebusch, and D.G. Ireland, Phys. Rev. C **75**, 045204 (2007).
- [20] A.V. Anisovich, R. Beck, E. Klempt, V.A. Nikonov, A.V. Sarantsev, and U. Thoma, Eur. Phys. J. A **48**, 15 (2012); <http://pwa.hiskp.uni-bonn.de/baryon.htm>
- [21] R. Shyam, O. Scholten and H. Lenske, Phys. Rev. C **81**, 015204 (2010).
- [22] V. Shklyar, H. Lenske and U. Mosel, Phys. Rev. C **72**, 015210 (2005).
- [23] F. Huang, M. Döring, H. Haberzettl, J. Haidenbauer, C. Hanhart, S. Krewald, U. G. Meißner and K. Nakayama, Phys. Rev. C **85**, 054003 (2012).
- [24] B. Borasoy, P.C. Bruns, U.-G. Meißner, and R. Nissler, Eur. Phys. J. A **34**, 161 (2007).
- [25] P. Vancraeyveld, Ph.D. thesis, Ghent University, 2011.
- [26] A. Starostin *et al.*, Phys. Rev. C **64**, 055205 (2001).
- [27] R. Novotny, IEEE Trans. Nucl. Sci. **38**, 379 (1991).
- [28] A.R. Gabler *et al.*, Nucl. Instrum. Methods A **346**, 168 (1994).
- [29] H. Herminghaus *et al.*, IEEE Trans. Nucl. Sci. **30**, 3274 (1983).
- [30] K.-H. Kaiser *et al.*, Nucl. Instrum. Methods A **593**, 159 (2008).
- [31] J.C. McGeorge *et al.*, Eur. Phys. J. A **37**, 129 (2008).
- [32] I. Anthony *et al.*, Nucl. Instrum. Methods A **310**, 230 (1991).
- [33] S.J. Hall *et al.*, Nucl. Instrum. Methods A **368**, 698 (1996).
- [34] S. Prakhov *et al.*, Phys. Rev. C **79**, 035204 (2009).
- [35] E.F. McNicoll *et al.*, Phys. Rev. C **82**, 035208 (2010).
- [36] R. Gatto, Phys. Rev. **109**, 610 (1958).
- [37] A. Sarantsev, J. Ryckebusch, and P. Vancraeyveld, private communication.